Design of Wide-Band (and Narrow-Band) Band-Pass Microwave Filters on the Insertion Loss Basis*

GEORGE L. MATTHAEI†, MEMBER, IRE

Summary—A method for design of band-pass microwave filters is described that combines the image and insertion-loss points of view to give an approximate design method having simplicity, but also high precision. This method is applicable for filter designs ranging from narrow to very wide bandwidths (2 to 1 or more). The desired insertion loss characteristic is obtained by use of a lumped-element, Tchebycheff, or maximally flat (or other) low-pass prototype. With the aid of the concept of impedance inverters, the prototype is converted into a cascade of symmetrical (but differing) sections. The image properties of symmetrical sections of the band-pass microwave filter structure are then related to those of corresponding sections of the prototype. Straightforward design equations are given for filters using short-circuited or open-circuited stubs, and also for filters using parallel-coupled lines. Mapping functions are derived that permit accurate prediction of the microwave filter cutoff characteristic from that of the prototype. The responses of a number of filter designs were computed, and a Tchebycheff filter with a 2.2 to 1 bandwidth was built and tested. The responses of all of the filter designs were in close agreement with the prescribed characteristics, and the accuracy of the mapping functions was verified.

I. Introduction

THE TYPES of band-pass filters to be treated in this paper are shown in Figs. 1–3. Filters using some of these structures have often been designed in the past using image design methods. Although these methods are conceptually simple, the over-all filter response to be expected is known only approximately, as a result of reflections at the terminating end sections. Thus, using such methods, it takes either a great deal of trial and error or a great deal of "know how" in order to obtain precision designs with specified pass band attenuation tolerances. Design methods, such as those discussed herein, on the insertion loss basis, have the advantage that the nature of the filter response can be specified at the outset of the design process, and the final filter design will closely adhere to the specifications.

The filter in Fig. 1(a) is of the parallel-coupled type for which Cohn[1] has presented approximate insertion-loss-basis design equations accurate for filters of narrow or moderate bandwidth; the filter form shown in Fig. 1(d) was previously treated by Jones[2] on an exact insertion-loss basis. It can be shown that exact design procedures using Richards' transformation[3] can be derived for all of these filters for either narrow or wide bandwidths. Examples of the use of these procedures will be found in the literature.[2,4–7] However, the paper by Jones,[2] which treats the form of filter in Fig. 1(d), is the only one of these references which deals specifically with any of the filters in Figs. 1(a) to 3 on an exact insertion-loss design basis. A serious practical disadvantage of exact methods for designing these particular filter structures is that the synthesis of special transfer functions is required[8] at the outset of the design process,[2] and, all in all, a great deal of computational labor is needed. Even though the design procedures described herein are computationally very simple and only approximate, the results, as the examples show, are satisfactory for most practical precision-design problems. Another advantage of the methods described herein is that they are quite flexible. As will be seen, the design procedure can be adapted to include changes in impedance level or special forms of structures, as required by special practical situations. These methods can also be used for other types of structures than those discussed herein.[9]

Easy-to-use approximate insertion-loss-basis design methods for band-pass microwave filters have existed for some time. However, these methods have in the past involved narrow-band approximations and as a result have rarely been accurate for bandwidths much

* Received by the PGMTT, May 8, 1960. This research was supported by the Signal Corps under Contract DA 36-039 SC-74862.

† Stanford Res. Inst., Menlo Park, Calif.

[1] S. B. Cohn, *et al.*, "Research on Design Criteria for Microwave Filters," Stanford Res. Inst., Menlo Park, Calif., Final Rept., SRI Project 1331, Contract DA 36-039 SC-64625, ch. 4; June, 1957. Also S. B. Cohn, "Parallel-coupled transmission line-resonator filters," IRE TRANS. ON MICROWAVE THEORY AND TECHNIQUES, vol. MTT-6 pp. 223–231; April, 1958.

[2] *Ibid.* (SRI Rept.), ch. 3. Also, E. M. T. Jones, "Synthesis of wide-band microwave filters to have prescribed insertion loss," 1956 IRE CONVENTION RECORD, pt. 5, pp. 119–128.

[3] P. I. Richards, "Resistor-transmission-line circuits," PROC. IRE, vol. 36, pp. 217–220; February, 1948.

[4] H. Ozaki and J. Ishii, "Synthesis of transmission-line networks and the design of UHF filters," IRE TRANS. ON CIRCUIT THEORY, vol. CT-2, pp. 325–336; December, 1955.

[5] H. Ozaki and J. Ishii, "Synthesis of a class of strip-line filters," IRE TRANS. ON CIRCUIT THEORY, vol. CT-5, pp. 104–109; June, 1958.

[6] A. I. Grayzel, "A synthesis procedure for transmission line networks," IRE TRANS. ON CIRCUIT THEORY, vol. CT-5, pp. 172–181; September, 1958.

[7] N. R. Welsh and E. S. Kuh, "Synthesis of Resistor-Transmission Line Networks," Electronics Res. Lab., University of California, Berkeley, Rept. No. 74, ONR Contract N7-onr-29529; July 15, 1958.

[8] In general, whether or not special transfer functions are required depends on the location of the frequencies of infinite attenuation inherent in the desired filter structure. By choosing certain filter structures, the more common transfer functions can be used (see footnotes 5 and 6). Such structures, however, may not always be the most convenient to fabricate.

[9] For example, the case of filters consisting of transmission lines coupled by series capacitors was treated in the report· G. L. Matthaei, "Research on Design Criteria for Microwave Filters," Stanford Res. Inst., Menlo Park, Calif., Tech. Rept. 6, SRI Project 2326, Contract DA 36-039 SC-74862; May, 1959.

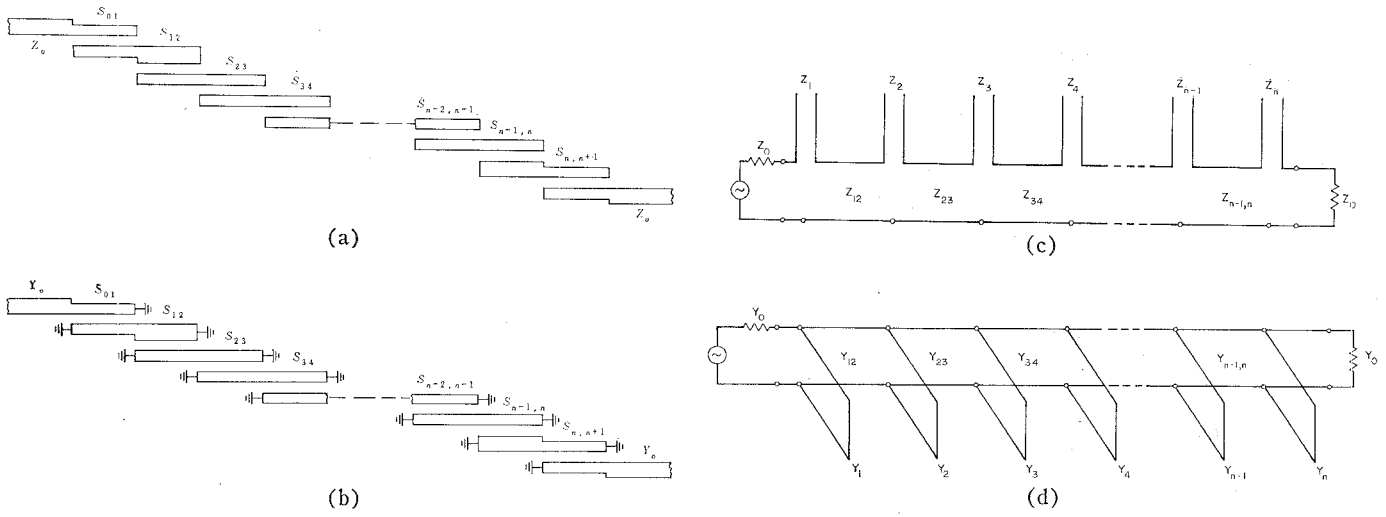

Fig. 1—(a) Parallel-coupled, strip-transmission-line filter with open-circuited sections. Each section is one-quarter wavelength long where the reference wavelength is that at the midband frequency, ω_0. Each section $S_{k,k+1}$ is characterized by even and odd mode impedances $(Z_{oe})_{k,k+1}$ and $(Z_{oo})_{k,k+1}$, respectively.[1,11,16] (b) Parallel-coupled, strip-transmission-line filter with short-circuited sections. This filter is the dual of that in (a). Each section $S_{k,k+1}$ is one-quarter wavelength long where the reference wavelength is the propagation wavelength at the midband frequency, ω_0. Each section $S_{k,k+1}$ is characterized by even and odd mode admittances $(Y_{oe})_{k,k+1}$ and $(Y_{oo})_{k,k+1}$, respectively.[11,16] (c) Band-pass filter using quarter-wavelength series stubs and quarter-wavelength connecting lines. Filters of the form in (a) can always be converted to this form. (d) Band-pass filter using quarter-wavelength shunt stubs and quarter-wavelength connecting lines. This filter is the dual of that in (c). The reference wavelength is the propagation wavelength at the midband frequency, ω_0.

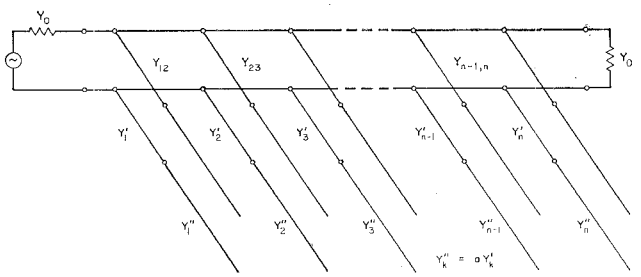

Fig. 2—Band-pass filter with half-wavelength shunt stubs and quarter-wavelength connecting lines. The reference wavelength is the propagation wavelength at the midband frequency, ω_0.

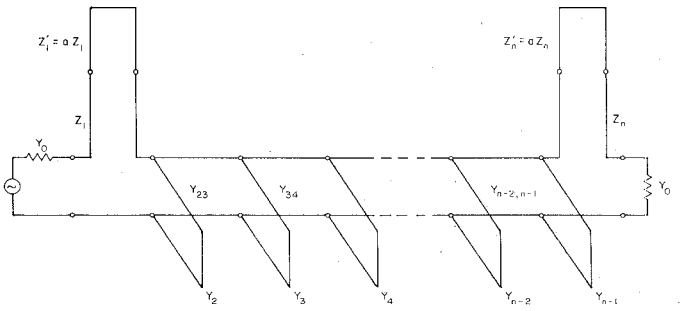

Fig. 3—Band-pass filter with quarter-wavelength shunt stubs, quarter-wavelength connecting lines, and half-wavelength series stubs at the ends. The reference wavelength is that at the midband frequency, ω_0.

over 20 per cent. The design approach used herein has the advantage that it does not involve approximations of a narrow-band sort; hence, it gives good accuracy for narrow bandwidths on out to bandwidths of 2 to 1 or more.

In Section II, the use of the design equations and the results of design examples will be discussed. To make routine use of the design equations more convenient, their derivation will be treated separately in Section III.

II. Practical Application of the Design Equations

A. Equivalence of the Networks in Figs. 1(a)–(d)

The filter in Fig. 1(b) is simply the dual of that in Fig. 1(a). It can be obtained directly from the circuit in Fig. 1(a) by replacing the open circuits by short circuits and by replacing each even- or odd-mode impedance, $(Z_{oe})_{k,k+1}$ and $(Z_{oo})_{k,k+1}$, respectively, by corresponding *odd-* and *even-mode* admittances.

$$(Y_{oo})_{k,k+1} = Y_0^2(Z_{oe})_{k,k+1},$$
$$(Y_{oe})_{k,k+1} = Y_0^2(Z_{oo})_{k,k+1}, \qquad (1)$$

where $Y_0 = 1/Z_0$ is the characteristic admittance of the input and output lines. By use of the equivalences shown in Fig. 4,[10,11] it is seen that the circuit in Fig. 1(c) is

[10] The correctness of these equivalences can be verified with the aid of the impedance and admittance matrices for parallel-coupled strips given by Jones and Bolljahn (see footnote 11) or by using Richards' viewpoint to map the elements in Equivalent Circuits (5) and (6) of Table II of Ozaki and Ishii's work (see footnote 5) into the corresponding transmission line form.

[11] Cohn, *et al.*, *op. cit.*, (SRI Rept.), ch. 4. Also, E. M. T. Jones and J. T. Bolljahn, "Coupled-strip-transmission-line filters and directional couplers," IRE Trans. on Microwave Theory and Techniques, vol. MTT-4, pp. 75–81; April, 1956.

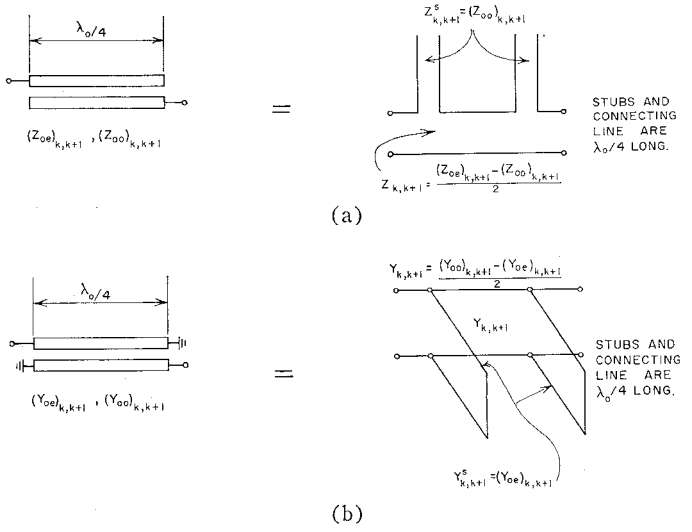

Fig. 4—Equivalence between parallel-coupled strip-line sections and sections consisting of stubs with connecting lines.

exactly equivalent to that in Fig. 1(a), while the circuit in Fig. 1(d) is exactly equivalent to that in Fig. 1(b). Thus, any of these four circuits can be derived from any other, by use of duality and the equivalences in Fig. 4; and when derived from one another in this manner, all will yield exactly the same transmission characteristic.

For simplicity, the design equations applicable for these four filter structures (Fig. 1) will be expressed in the specific form for the structure in Fig. 1(a). Any of the other forms may then be obtained by duality and Fig. 4. In converting from the form in Fig. 1(a) to the form in Fig. 1(d), for example, it should be noted that the characteristic admittance of the shunt stub at each end is determined solely by the end sections of the filter in Fig. 1(a); however, the characteristic admittance of each of the shunt stubs in the interior of the filter in Fig. 1(d) is determined by the corresponding two adjacent sections in Fig. 1(a) so that

$$\begin{aligned} Y_k &= Y^s_{k-1,k} + Y^s_{k,k+1} \\ &= Y_0{}^2[Z^s_{k-1,k} + Z^s_{k,k+1}] \\ &= Y_0{}^2[(Z_{oo})_{k-1,k} + (Z_{oo})_{k,k+1}], \end{aligned} \tag{2}$$

where $Y_0 = 1/Z_0$ is again the characteristic admittance of the input and output lines, and the $Y_{k,k+1}{}^s$ and $Z_{k,k+1}{}^s$ are defined in Fig. 4. It is helpful to note that in the case of Fig. 1(d), the characteristic admittances of the connecting lines are given by

$$Y_{k,k+1} = Y_0{}^2\left[\frac{(Z_{oe})_{k,k+1} - (Z_{oo})_{k,k+1}}{2}\right] = Y_0{}^2K_{k,k+1}, \tag{3}$$

where the $K_{k,k+1}$ are impedance inverter parameters to be discussed later. (They are defined numerically in Tables I and II, p. 592.)

The filter structures in Figs. 2 and 3 are not equivalent to those in Fig. 1; however, they are closely related structures which can readily be treated using many of the same concepts and equations.

B. Use of Mapping Functions, and Selection of Appropriate Lumped-Element Prototypes

In the design procedure described herein, the band-pass microwave filter derives characteristic properties of its response from a lumped-element prototype filter having analogous low-pass filter response properties. Fig. 5 shows a typical low-pass prototype and defines the prototype parameters $g_0, g_1 \cdots, g_n, g_{n+1}$. The design equations in Tables I–III (p. 592) assume that the prototype filter is either symmetric or antimetric[12]—a condition satisfied by the common maximally flat or Tchebycheff lossless filter designs (which have one or more frequencies at which zero reflection occurs).

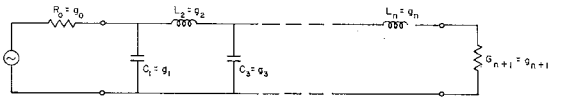

Fig. 5—Definition of the low-pass prototype parameters $g_0, g_1, \cdots, g_n, g_{n+1}$. The symmetry about the middle of the filter indicated in the equations of Tables I–III results from the use of symmetric or antimetric prototypes. The common maximally flat or Tchebycheff prototypes, which have one or more frequencies where zero reflection occurs, always satisfy this symmetry or antimetry condition.

A typical low-pass prototype is shown. The dual of this circuit would also be satisfactory.

$$g_k\,|_{k=1 \text{ to } n} = \begin{cases} \text{The inductance of a series coil, or the capacitance} \\ \text{of a shunt capacitor.} \end{cases}$$

$$g_0 = \begin{cases} \text{The generator resistance } R_0 \text{ if } g_1 = C_1, \text{ but is de-} \\ \text{fined as the generator conductance } G_0 \text{ if } g_1 = L_1. \end{cases}$$

$$g_{n+1} = \begin{cases} \text{The load resistance } R_{n+1} \text{ if } g_n = C_n, \text{ but is defined} \\ \text{as the load conductance } G_{n+1} \text{ if } g_n = L_n. \end{cases}$$

Note: An additional prototype parameter ω_1' is defined in Figs. 6 and 7.

Weinberg[13] and Technical Report 4 of this project[14] give tables of element values for such filters. (Weinberg[13] also includes tables for filters which are not symmetric or antimetric.) The use of symmetric or antimetric prototypes along with equal terminations in the final microwave filter (as depicted in Figs. 1–3) is usually desirable, and so has been made implicit in the equations in Tables I–III. However, these conditions are not

[12] E. A. Guillemin, "Synthesis of Passive Networks," John Wiley and Sons, Inc., New York, N. Y., p. 371; 1957.

[13] L. Weinberg, "Network Design by Use of Modern Synthesis Techniques and Tables," Res. Labs., Hughes Aircraft Co., Culver City, Calif., Tech. Memo. 427; April, 1956. Also, in *Proc. NEC*, vol. 12; 1956.

[14] W. J. Getsinger, *et al.*, "Research on Design Criteria for Microwave Filters," Stanford Res. Inst., Menlo Park, Calif., Tech. Rept. 4, SRI Project 2326, Contract DA 36-039 SC-74862; December, 1958.

necessary, and equations for other cases may be derived by the theory in Section III.

Fig. 6 shows a typical lossless low-pass-filter maximally flat response along with the equation for this response. The frequency ω_1' establishes the pass-band edge, while A_m is the db attenuation which is permissible within the pass band. The frequency ω_a' is a frequency at which a stated attenuation, A_a db, is required. An analogous maximally flat band-pass response, such as might be obtained by the filters in Fig. 1, is also shown. Note that this response has arithmetic symmetry about ω_0, so that the essential parameters of the respone may be specified simply as ω_1/ω_0, A_m, A_a, and ω_a/ω_0. The response of the band-pass filter may be predicted directly from that of the low-pass filter by mapping the ω' frequency scale of the low-pass filter to the ω frequency scale of the band-pass filter, as indicated in the figure. For the circuits in Fig. 1, and the design equations in Tables I and II, the proper function $F_n(\omega/\omega_0)$ to use is

$$F_n\left(\frac{\omega}{\omega_0}\right) = \frac{-\cos\left(\frac{\pi}{2}\,\frac{\omega}{\omega_0}\right)}{\sqrt[n]{\left|\sin\left(\frac{\pi\omega}{2\omega_0}\right)\right|}}. \tag{4a}$$

For narrow or moderate bandwidths, the simpler function

$$F_n\left(\frac{\omega}{\omega_0}\right) = \left(\frac{\omega}{\omega_0} - 1\right) \tag{4b}$$

will also give good accuracy.[1] As will be shown, the accuracy of (4b) is fair even for wide bandwidths. For the circuit in Fig. 3 and the equations in Table III, the proper function to use is

$$F_n\left(\frac{\omega}{\omega_0}\right) = \frac{-\cos\left(\frac{\pi\omega}{2\omega_0}\right)}{\sqrt[n]{\left|\sin\left(\frac{\pi\omega}{2\omega_0}\right)\right|\left[\sin\left(\frac{\pi}{2}\,\frac{(\omega-\omega_\infty)}{(\omega_0)}\right)\right]^2\left[\sin\frac{\pi}{2}\left(\frac{(\omega-2\omega_0+\omega_\infty)}{(\omega_0)}\right)\right]^2}}, \tag{5}$$

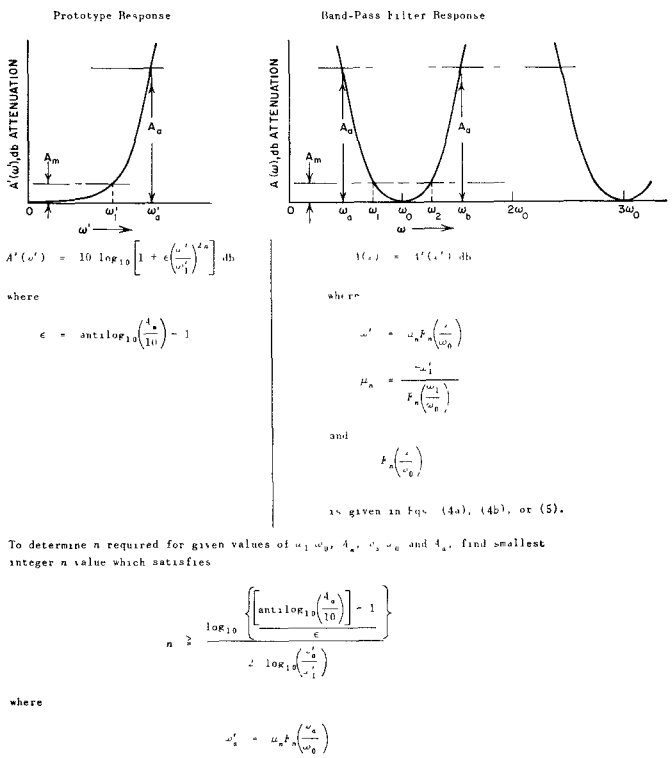

Fig. 6—Equations and parameters for maximally flat response.

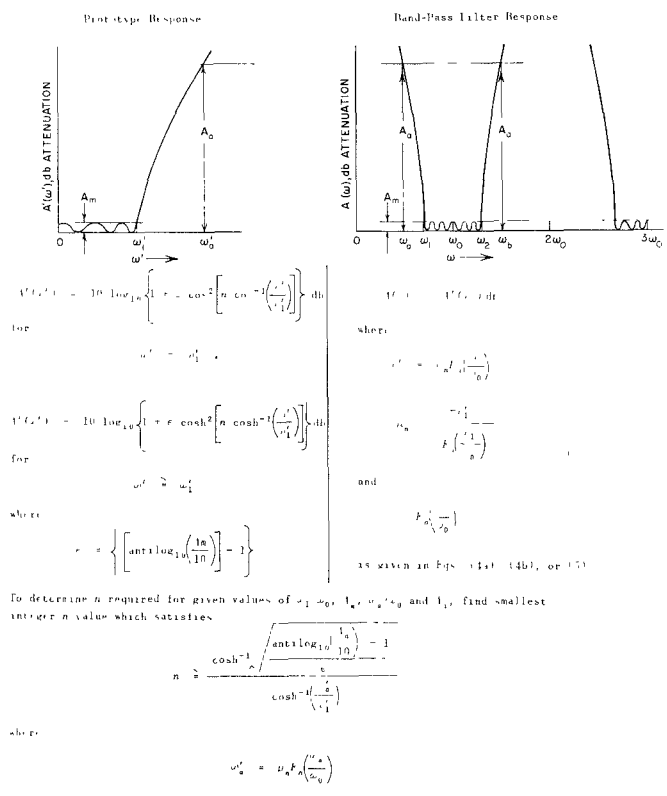

Fig. 7—Equations and parameters for Tchebycheff response.

where ω_∞ is a frequency of infinite attenuation, to be specified. An accurate general mapping for the circuit in Fig. 2 has not been determined.

Fig. 7 shows corresponding curves and equations for the case of filters having Tchebycheff responses. Since the choice of mappings is determined by the type of filter structure, rather than by the type of response, the functions in (4) and (5) apply as before. For both the maximally flat and Tchebycheff cases, the number of reactive elements n required in the low-pass prototype is fixed by the parameters ω_1/ω_0, A_m, ω_a/ω_0, and A_a. In Figs. 6 and 7, equations are given for solving for n in terms of these parameters. Since the $F_n(\omega_a/\omega_0)$ in (4a) and (5) are also functions of n, one must estimate a value of n to use in these functions, solve for n to get an improved value, and then repeat the process. However, since the $F_n(\omega_a/\omega_0)$ are only weak functions of n, the process will converge very quickly. In the case of (4a) and (4b), the latter equation may be easily used to obtain n accurately for narrow-band cases, and this equation will also give a fairly accurate value of n in wide-band cases. In wide-band cases, the value of n obtained using (4b) can be inserted in (4a), and the equation for n can then be used again to obtain a more accurate verification of the n value.

C. A Design Procedure Especially Suited to Filters Realized in the Forms in Fig. 1(a) and (b)

Table I summarizes a design procedure which gives good impedance levels for filter structures such as those in Fig. 1(a) and (b). After an appropriate prototype is selected, as described above, the parameters g_0, g_1, $\cdots$, g_n, g_{n+1}, and ω_1' from the low-pass prototype are used along with the band-pass-filter lower-band-edge ratio, ω_1/ω_0, to obtain the filter design in a straightforward manner as outlined.

Fig. 8 shows the results of some trial designs obtained by using a Tchebycheff prototype having 0.10-db pass band ripple and $n=6$ reactive elements. The curves show the response, computed by a digital computer, from the circuit element values. For Fig. 8(a), $\omega_1/\omega_0 = 0.975$ was used, which calls for a 5 per cent bandwidth. As is seen from the figure, there is no noticeable deviation from the design objective, and points mapped from the low-pass prototype response by use of (4a) and also by (4b) are all in excellent agreement with the computed response. Fig. 8(b) shows the computed response for a design obtained using $\omega_1/\omega_0 = 0.850$, which calls for a 30 per cent bandwidth. In this case, there is a very slight deviation from perfect Tchebycheff character, inasmuch as two of the peaks of the pass band ripples do not quite reach the 0.10-db level. In this case, points mapped from the prototype response using (4a) are in practically perfect agreement with the filter response, while points mapped using (4b) show some noticeable error at the higher attenuation levels.

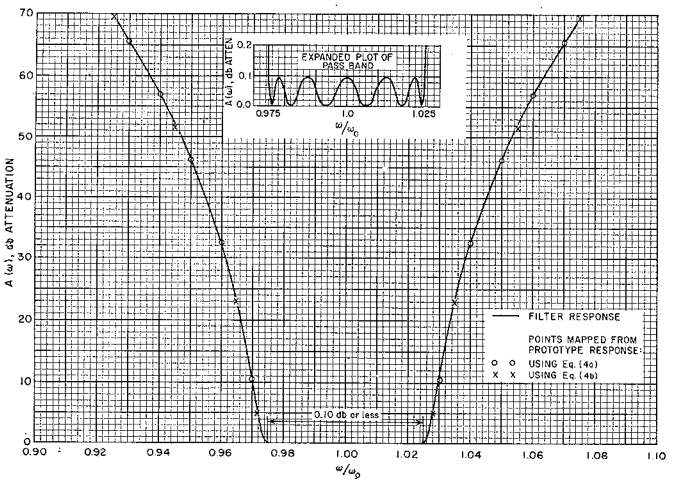

(a)

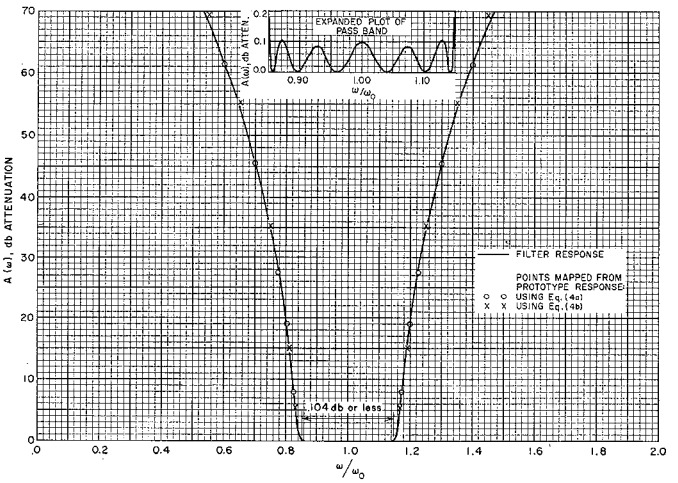

(b)

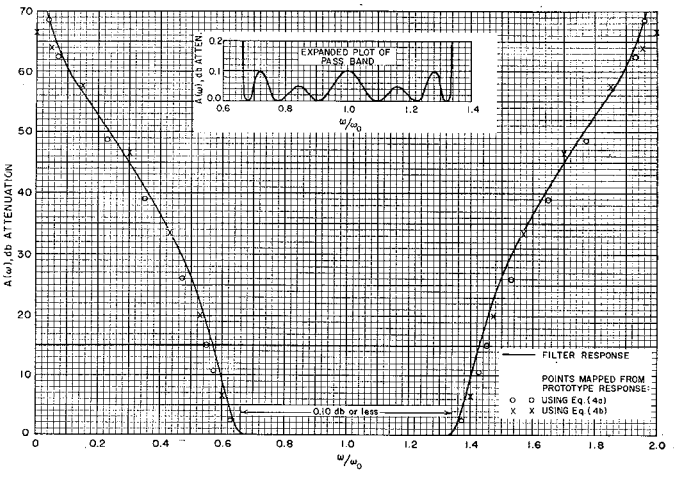

(c)

Fig. 8—(a) Computed response of filter designed as in Table I to have 5 per cent bandwidth. Design value for ω_1/ω_0 was 0.975. Prototype had 0.10-db Tchebycheff pass band ripple with $n=6$ reactive elements). (b) Computed response of filter designed as in Table I to have 30 per cent bandwidth. Design value of ω_1/ω_0 was 0.850. Prototype same as (a). (c) Computed response of filter designed as in Table 1 to have approximately 2 to 1 bandwidth. Design value for ω_1/ω_0 was 0.650, which calls for $\omega_2/\omega_1 = 2.077$. Prototype same as for (a).

Fig. 8(c) shows the computed response for a design obtained using $\omega_1/\omega_0=0.650$, which calls for a band-edge ratio of $\omega_2/\omega_1=2.077$. In this case, the deviation from a perfect response is more noticeable, the most important deviation being that the frequency ratio of the 0.10-db band-edge points is about $\omega_2/\omega_1=1.96$, instead of 2.077. All of the expected pass band ripples are present, although in this case two of the ripple peaks are reduced to half size. Points mapped from the prototype response by use of (4a) appear to fall almost exactly where the response curve would have been if the slight shrinkage in the pass band width had not occurred. Points mapped by use of (4b) weave across the computed response somewhat, but follow it surprisingly closely.

Table IV (p. 593) gives the odd- and even-mode impedances[11] for these filters realized in the form in Fig. 1(a). Using construction methods to be outlined later, all three of these designs should be quite practical. Filters designed by use of Table I and realized in the form in Fig. 1(a) or (b), are of special practical interest for applications where bandwidths of perhaps 50 per cent or less are desired. Although the forms in Fig. 1(a) and (b) are also practical for larger bandwidths, filters designed by Table II and realized in the form in Fig. 1(d) will have reasonable element values for large bandwidth designs and become attractive because they require two less sections to achieve a given response.

A corresponding filter designed by Cohn's equations[1] was compared with the 5 per cent bandwidth filter described herein, in order to compare the two design methods. The designs were found to be basically similar, except that Cohn's equations yielded slightly different end sections and a 7 per cent higher impedance level in the interior sections of the filter. For filters of about 10 per cent bandwidth or less, either method should give good designs, but Cohn's design method has an advantage of being computationally even simpler than that described herein. For bandwidths greater than about 10 or 15 per cent, the accuracy of Cohn's equations begins to deteriorate noticeably and the design equations described herein are preferable.

D. A Design Procedure Especially Suited to Filters Realized in the Forms in Figs. 1(c) and (d)

In the design procedure of Table I, the end sections S_{01} and $S_{n,n+1}$ are, in a sense, primarily impedance-transforming sections. Using that design procedure, moderate impedance levels are maintained in the interior sections of filters realized in the forms in Figs. 1(a) or (b), regardless of the bandwidth of the filter, but this is achieved by not making full use of all of the natural modes of oscillation of which the circuit is capable. Using the design procedure in Table II, the end sections S_{01} and $S_{n,n+1}$ are eliminated, and the remaining network makes full use of all possible natural modes. Table II is thus seen to call for $n-1$ band-pass filter sections to realize a response mapped from an n-reactive-element prototype, while the design method in Table I calls for $n+1$ band-pass filter sections to achieve the same response. Designs obtained by Table II will usually yield impractical impedance levels for filters of the forms in Fig. 1(a) and (b), but the impedance levels are moderate for wide-band filters of the forms in Fig. 1(c) and (d). The form in Fig. 1(d), which is quite practical for wide-band designs, becomes less practical for narrow-band designs since the characteristic admittances of the shunt stubs then become quite large.

Fig. 9 shows the response of a filter designed using Table II from a 0.10-db ripple, $n=8$, Tchebycheff prototype with $\omega_1/\omega_0=0.650$. Table V (p. 593) shows the element values for a realization as in Fig. 1(d). In this case, the pass band ripples are more uneven than in the previous examples; however, the bandwidth suffered less shrinkage than in the previous 2 to 1 bandwidth design, whose response was shown in Fig. 8(c). In both the case of Fig. 8(c) and the case of Fig. 9, the filter has seven sections; however, it should be noted that the latter response has a steeper cutoff, since it was designed from an $n=8$ instead of an $n=6$ prototype. It is thus seen that points mapped from the prototype response by use of (4a) are again quite accurate, but those using (4b) show appreciable error at high attenuation levels.

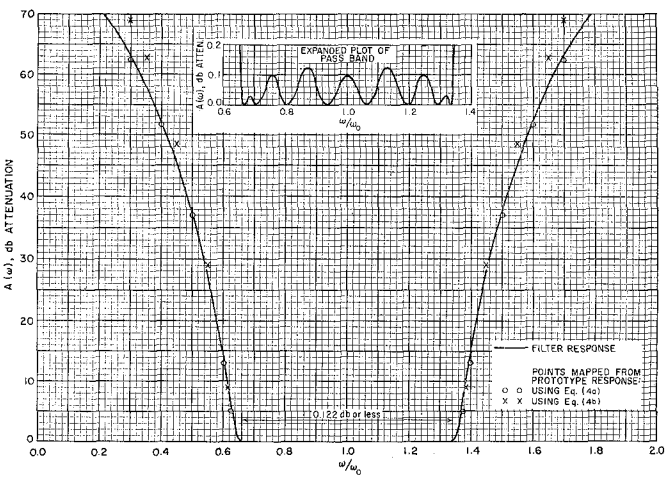

Fig. 9—Computed response of a filter designed as in Table II to have approximately 2 to 1 bandwidth. Design value for ω_1/ω_0 was 0.650. Prototype had 0.10-db Tchebycheff pass band ripple with $n=8$ reactive elements.

If filters in the form of Fig. 1(c) or 1(d) are desired, but with a somewhat different impedance level for their interior sections, they can be achieved by using a modified form of the calculation procedure in Table III, as is described in Section III-D.

E. Design of Filters in the Form in Fig. 2

Filters of the form shown in Fig. 2 can be readily designed by a modified use of Table II. The design is

carried out to first give a filter in the form in Fig. 1(d), with the desired pass band characteristic and bandwidth. Then each shunt, quarter-wavelength,[15] short-circuited stub of characteristic admittance Y_k is replaced, as shown in Fig. 2, by a shunt, half-wavelength, open-circuited stub having an inner quarter-wavelength portion with a characteristic admittance,

$$Y_k' = \frac{Y_k(a \tan^2 \theta_1 - 1)}{(a + 1) \tan^2 \theta_1}, \tag{6}$$

and an outer quarter-wavelength portion with a characteristic admittance,

$$Y_k'' = a Y_k'. \tag{7}$$

The parameter a is fixed by

$$a = \cot^2 \left(\frac{\pi \omega_\infty}{2\omega_0} \right) \Bigg|_{(\omega_\infty/\omega_0) < (\omega_1/\omega_0)}, \tag{8}$$

where $\theta_1 = \pi\omega_1/2\omega_0$, and ω_∞ is a frequency at which the shunt lines present short circuits to the main line and cause infinite attenuation. The principle upon which the above substitution is made is that (6) to (8) are constrained to yield half-wavelength open-circuited stubs, which have exactly the same susceptance at the band-edge frequency ω_1, as did the quarter-wavelength short-circuited stubs that they replace, while both kinds of stubs have zero admittance at ω_0.

To test out this procedure, a filter was designed as in Table II to give 30 per cent bandwidth ($\omega_1/\omega_0 = 0.850$) using a 0.10-db Tchebycheff prototype with $n = 8$. Then, choosing $\omega_\infty/\omega_0 = 0.500$, which gives $a = 1$, the quarter-wavelength stubs were replaced by half-wavelength stubs as described above, and the resulting computed response is shown in Fig. 10. Note that the pass band is almost exactly as prescribed, and that there are low attenuation regions in the vicinity of $\omega = 0$ and $\omega = 2\omega_0$, which are to be expected. The element values for this filter are shown in Table VI (p. 593).

The 2 to 1 bandwidth filter design (Fig. 9 and Table V) was also converted to this form using $\omega_\infty/\omega_0 = 0.500$, and its response was computed. The features of the pass band looked much the same as those in the expanded plot in Fig. 9, while the stop bands consisted of very sharp attenuation spikes surrounding $\omega/\omega_0 = 0.500$, in a manner similar to that in Fig. 10, except that the attenuation bands were much narrower.

Filters of the form in Fig. 2 should be particularly useful where the pass bands around $\omega = 0$ and $\omega = 2\omega_0$ are not objectionable, and where there is a relatively narrow band of signals to be rejected. By the proper choice of ω_∞, the infinite attenuation point can be placed so as to give maximum effectiveness against the unwanted signals. Filters of the form in Fig. 2 are more practical for narrower bandwidths than are those in the form in Fig. 1(d), because of the larger susceptance slope of half-wavelength stubs for a given characteristic admittance. For example, in the case of Fig. 10, the shunt stubs for this filter as shown in Fig. 2 have characteristic admittances $Y_k' = Y_k''$, which are 0.471 times the characteristic admittances of the shunt stubs of the analogous filter in the form in Fig. 1(d), from which it was designed. Thus narrower bandwidths can be achieved without having the characteristic admittances of the shunt stubs become excessive.

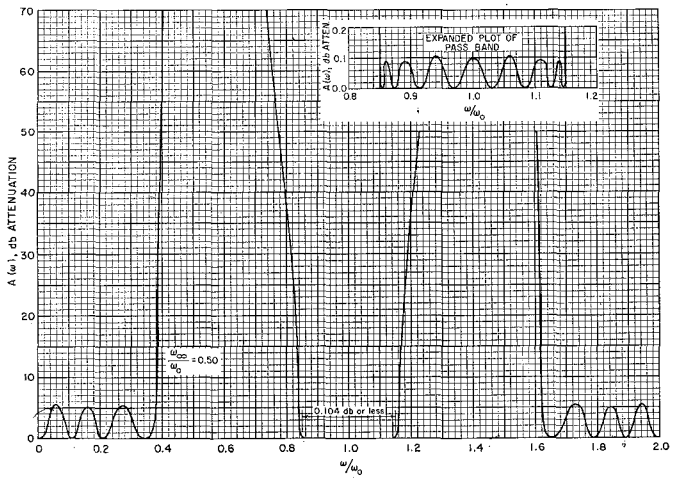

Fig. 10—Computed response of a 30 per cent band-pass filter designed in the form in Fig. 2. Design value for $\omega_1/\omega_0 = 0.850$. Prototype had 0.10-db Tchebycheff ripple with $n = 8$ reactive elements.

F. Design of Filters in the Form in Fig. 3

For filters of the form in Fig. 3, the mapping function in (5) should be used along with the equations in Table III. In this case ω_∞ is the frequency of infinite attenuation created by the half-wavelength series stubs at the ends. The parameter d may be chosen to adjust the impedances of the interior of the filter to a convenient level.

This type of filter gives a cross between the type of response obtained using a filter as in Fig. 1(d), and that obtained by a filter as in Fig. 2. At first, a design of the form in Fig. 1(d) was tried, but with the end stubs (only) replaced with shunt half-wavelength open-circuited stubs. This gave infinite attenuation at $\omega = 0$ and ω_∞ as expected, but yielded a point of very low attenuation (around 10 db) between these two frequencies (and between other corresponding frequencies). It was then found that by using an altered design procedure which yields series half-wavelength short-circuited stubs at the ends, the desired type of response could be obtained without excessive drop in attenuation between $\omega = 0$ and ω_∞.

[15] The reference wavelength is that at the mid-band frequency ω_0

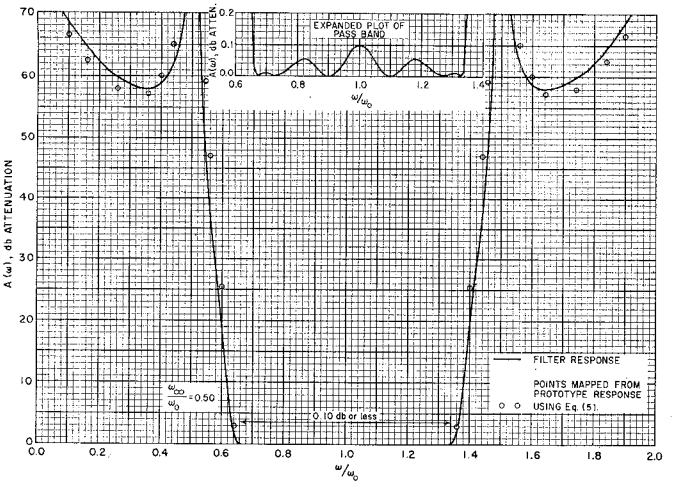

Fig. 11—Computed response of a filter as in Fig. 3, with approximately 2 to 1 bandwidth. Design value for ω_1/ω_0 was 0.650. Prototype had 0.10-db Tchebycheff ripple with $n=8$ reactive elements. Parameters d and ω_∞/ω_0 were both chosen as 0.500.

Fig. 11 shows the computed response of a filter designed using Table III to give approximately 2 to 1 bandwidth. The prototype, again, had 0.10-db Tchebycheff ripple, and $n=8$. The remaining design parameters were $\omega_1/\omega_0=0.650$, $\omega_\infty/\omega_0=0.500$, and $d=0.500$. In this case the pass band ripples are not as well developed as in the previous examples. It has been found that the design theory used herein works best if all of the sections are of the same basic form; since the end sections are different from the other sections in this case, the larger deviation from a 0.10-db equal-ripple response is not surprising. (From a practical standpoint, this deviation may be good, since the ripples are small at the band edges, where incidental dissipation will tend to increase the pass band loss most.) Points mapped from the prototype response using (5) are seen to come fairly close to the computed response, although not as close as (4a) did where it was applicable. Both (4a) and (5) were derived on the same basis and should probably yield similar accuracy. The larger deviations in this case are probably due at least in part to the fact that the pass band response itself deviates more from the design objective. The element values for this filter design are given in Table VII (p. 593).

G. Suggested Ways for Fabricating the Filters Under Consideration

For bandwidths of perhaps around 20 per cent or less, filters of the form in Fig. 1(a) are readily realized in printed-circuit form by use of Cohn's data for zero-thickness parallel-coupled strips.[1,16] Larger bandwidths are difficult using this construction, because the gaps between the conductors must become extremely small. A suggested way for getting around this problem while still using printed circuit construction is shown in Fig. 12. Instead of just two slabs of dielectric, four slabs are used, two of which are relatively thin. Then alternate conductors are printed to form a double layer, as shown in the cross-sectional view, so that the adjacent conductors can be interleaved. This gives a relatively large odd-mode capacitance without the need for extremely close spacings. The cross section of the conductors is no longer balanced geometrically; however, by proper design, the even- and odd-mode impedances for both the single- and double-layer conductors can be made the same.

Fig. 13 shows a suggested way for realizing filters of the type in Fig. 1(b). In this case, the conductors are rectangular bars supported mechanically by the short circuits at their ends. This construction can be used for either narrow- or wide-band filters and has the advantages of not requiring dielectric material (hence having no dielectric loss), and, with rounded corners on the conductors, of having relatively high power-handling capability.

Fig. 14(a) shows a possible way for building filters of the type in Fig. 1(d). This filter uses mostly double stubs instead of single stubs, so that the cross-sectional dimensions of the stubs (and the junction discontinuities) can be made smaller. It was designed in thick bar strip-line construction, in order to reduce the junction discontinuity effects and to make these effects less frequency-sensitive.[17] This filter was designed for a 2.2 to 1 bandwidth from a 0.10-db Tchebycheff ripple ten-reactive-element prototype. Three additional sections identical with the middle sections of the $n=10$ design were added in order to increase the rate of cutoff. This gave a resulting design which is not quite the same as a true $n=13$, 0.10-db-ripple Tchebycheff design, but the difference is small. As can be seen from the measured results in Fig. 14(b), the response is close to the theoretical.

It has been observed that any of the types of filters in Figs. 1, 2, or 3 may have narrow spurious pass bands, at frequencies in the vicinity of $f=2f_0$, if there is deviation from perfect tuning in one part of a filter with respect to the rest of the filter. Since small deviations from perfect tuning are difficult to avoid, some measures should be taken to suppress these spurious pass bands if they are objectionable for the application

[16] S. B. Cohn, *et al.*, "Strip Transmission Lines and Components," Stanford Res. Inst., Menlo Park, Calif., Final Rept., SRI Project 1114, Contract DA-36-039 SC-63232, ch. 3; February, 1957. Also, S. B. Cohn, "Shielded coupled-strip transmission line," IRE TRANS. ON MICROWAVE THEORY AND TECHNIQUES, vol. MTT-3, pp. 29–38; October, 1955.

[17] P. S. Carter, Jr., G. L. Matthaei, and W. J. Getsinger, "Design Criteria for Microwave Filters and Coupling Structures," Stanford Res. Inst., Menlo Park, Calif., Tech. Rept. 8, pt. 3, SRI Project 2326, Contract DA 36-039 SC-7462. This reference discusses reasons why this bar construction is expected to have less junction discontinuity effect than either thin strip transmission line or coaxial line construction of equivalent size. It also discusses other practical matters with respect to the design of this type of filter.

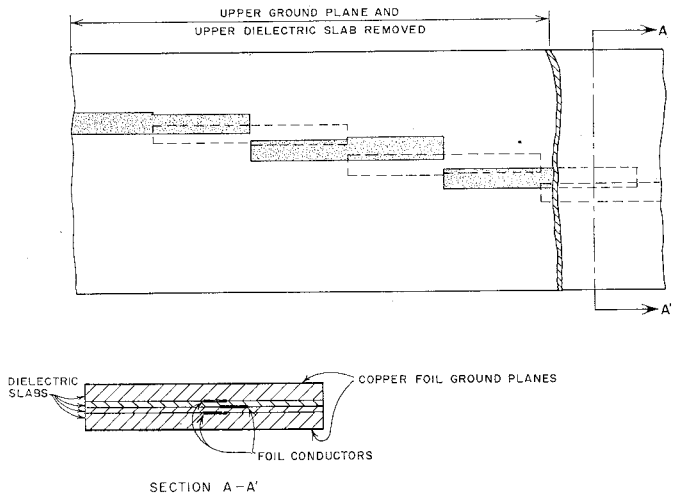

Fig. 12—Possible means for fabricating wide-band filters of the type in Fig. 1(a), using printed circuit techniques. (In order to achieve tight coupling with reasonably large conductor spacings, alternate conductor strips are made to be double so that conductor strips can be interleaved. This construction is electrically balanced with respect to the ground planes and will not excite ground plane modes, as would overlapped strips which did not interleave.)

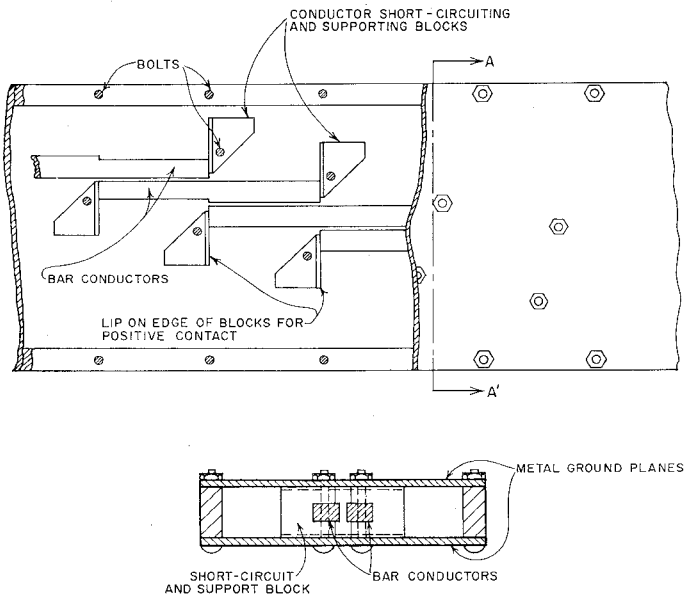

Fig. 13—Possible means for fabricating wide-band filters of the type in Fig. 1(b), in bar-transmission-line construction. (The short-circuiting blocks support the bar conductors so that no dielectric material is required.)

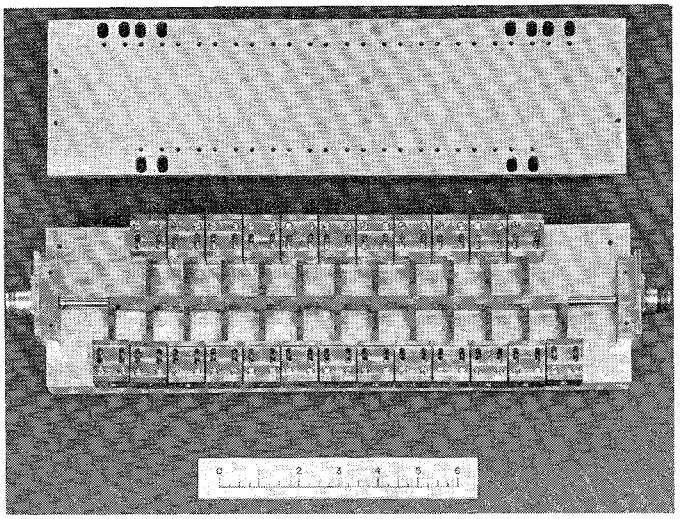

(a)

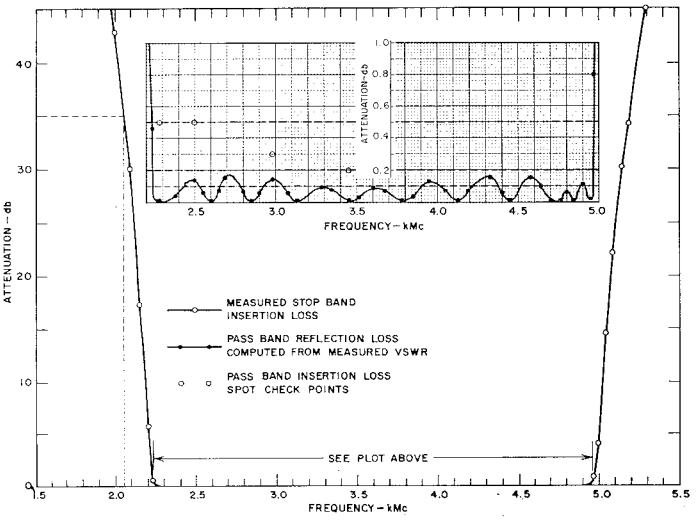

(b)

Fig. 14—(a) Filter of the type in Fig. 1(d) with cover plate removed. Rectangular bar strip transmission line construction is used. The blocks along the sides of the filter short circuit the stubs and support the center-conductor structure. (b) Measured response of the filter in Fig. 14(a). The dissipation loss can be reduced by silver plating since the filter as tested used a brass inner structure with aluminum cover plates.

at hand. A possible way of suppressing such responses is to use a filter of the form in Fig. 3, with $a = \infty$, so that the series stubs become open-circuited stubs one-quarter-wavelength long at f_0. Although this has not been tested as yet, it appears reasonable that series stubs of this sort can be used to maintain high attenuation in the vicinity of $2f_0$, since they present large series reactances at frequencies in the vicinity of $2f_0$, while the spurious responses in the shunt-stub portion of the filter are due to large shunt susceptances of opposite signs cancelling each other. Quarter-wavelength or half-wavelength series stubs, such as those in Fig. 3, can be realized as coaxial structures within the center conductor of the filter.[6]

III. Theoretical Basis for the Filter Equations and Mapping Functions

A. Modified Prototypes as a Basis for Design

The first step in deriving the design equations used herein is to convert the low-pass prototype (Fig. 5) to a modified form that involves impedance inverters or admittance inverters. The concept of impedance inverters has previously been discussed in detail by

Cohn;[18] admittance inverters are simply the dual representations of impedance inverters, and are introduced only for convenience. Fig. 15 summarizes the basic properties of these two types of inverters.

Using methods similar to those of Cohn,[18] any circuit like that in Fig. 5 may be converted into either of the dual forms in Fig. 16. In Fig. 16(a), which uses impedance inverters, all of the elements R_g, L_{a1}, L_{a2}, $\cdots$, L_{an}, R_L may be chosen arbitrarily; the inverter parameters $K_{k,k+1}$ are then computed as indicated.

Analogous conditions hold for the dual circuit at (b) in Fig. 16. In the discussion to follow, the impedance (or admittance) inverters will be assumed to be idealized so that their electrical behavior is exactly as indicated in Fig. 15. They will be used merely as an aid to mathematical reasoning, and no direct attempt will be made to find a circuit which approximates their idealized performance. Instead, as indicated below, the approximations will be based upon the impedance inverters plus part of each adjacent element.

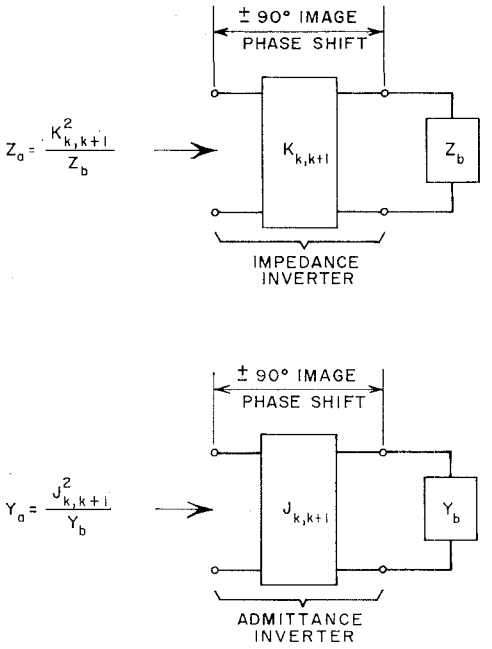

Fig. 15—Definition of impedance inverters and admittance inverters.

B. *Procedure for Deriving the Equations in Table I*

The design equations in Table I are based on the modified prototype shown at (a) in Fig. 16, while Fig. 17 shows the manner in which the element values are specified, and the manner in which the prototype is broken into sections. The image impedance, $Z^i_{k,k+1}(\omega')$, and phase, $\beta_{k,k+1}$ (in the pass band) for each of the prototype interior sections (S_{12}' to $S_{n-1,n}'$) are readily shown to be

$$Z^i_{k,k+1}(\omega') = K_{k,k+1}\sqrt{1-\left(\frac{\omega'(L_a/2)}{K_{k,k+1}}\right)^2} \tag{9}$$

and

$$\beta_{k,k+1} = \Big|_{\omega' \leqq (K_{k,k+1})/(La/2)} = \sin^{-1}\left[\frac{\omega'(L_a/2)}{K_{k,k+1}}\right] \pm \frac{\pi}{2}, \tag{10}$$

where, as before, ω_1' is the cutoff frequency for the low-pass prototype. The choice of $\pm\pi/2$ in (10) depends on whether the inverter is taken to have ± 90 degrees phase shift. The work of Jones and Bolljhan shows[11] that the image impedance and pass band image phase for a parallel-coupled section as shown in Fig. 4(a) are given by

$$Z_I = \frac{\sqrt{(Z_{oe}-Z_{oo})^2 + (Z_{oe}+Z_{oo})^2\cos^2\theta}}{2\sin\theta} \tag{11}$$

and

$$\beta = \cos^{-1}\left[\left(\frac{Z_{oe}+Z_{oo}}{Z_{oe}-Z_{oo}}\right)\cos\theta\right], \tag{12}$$

where $\theta = \pi\omega/2\omega_0$, and where Z_{oe} and Z_{oo} are the even- and odd-mode line impedances, respectively. The

[18] Cohn, *et al.*, *op. cit.*, footnote 1 (SRI Rept.), ch. 2. Also, S. B. Cohn, "Direct-coupled-resonator filters," PROC. IRE, vol. 45, pp. 187–196; February, 1957.

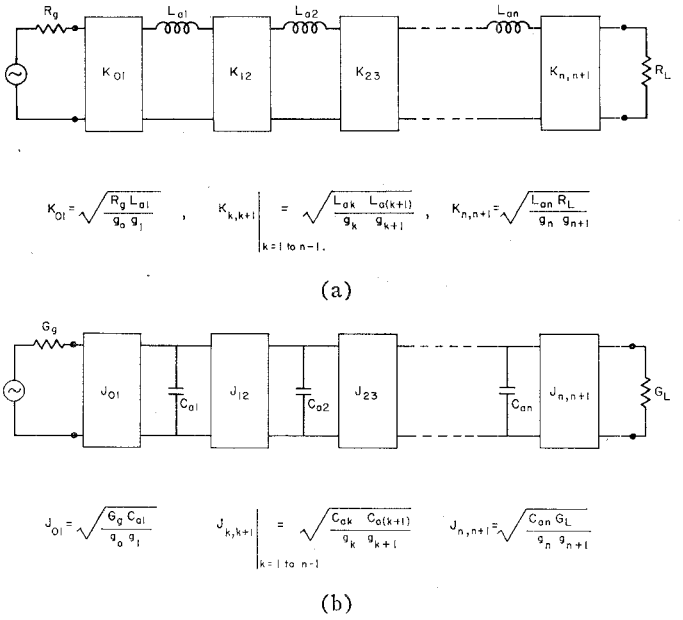

Fig. 16—Low-pass prototypes modified to include impedance inverters or admittance inverters. (The g_0, g_1, $\cdots$, g_n, g_{n+1} are obtained from the original prototype as in Fig. 5, while the R_g, L_{a1}, $\cdots$, L_{an}, and R_L or the G_g, C_{a1}, $\cdots$, C_{an}, and G_L may be chosen as desired.) (a) modified prototype using impedance inverters. (b) Modified prototype using admittance inverters.

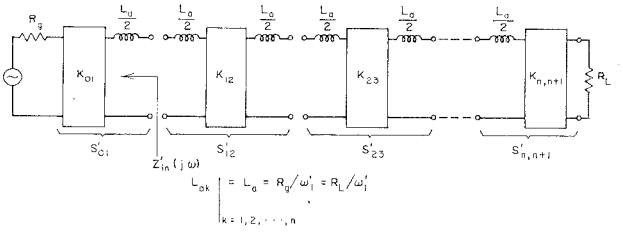

Fig. 17—Modified prototype for deriving the design equations in Table I.

parameters of the parallel-coupled sections S_{12} to $S_{n-1,n}$ in Fig. 1(a) are related to the prototype sections S_{12}' to $S_{n-1,n}$ of the prototype by forcing the following correspondences between the two structures:

(a) The image phase of the parallel-coupled sections when $\omega=\omega_0$ must be the same as the image phase of the prototype sections when $\omega'=0$.

(b) The image impedances of the parallel-coupled sections when $\omega=\omega_0$ must be the same (within a scale factor s)[19] as the image impedances of the corresponding prototype sections when $\omega'=0$.

(c) The image impedance of the parallel-coupled sections when $\omega=\omega_1$ must be the same (within a scale factor s)[19] as the image impedances of the corresponding prototype sections when $\omega'=\omega_1'$. (13)

Correspondence (a) is fulfilled in this case by choosing the + sign in (10). Equating (9) and (11) and evaluating each side at the appropriate frequencies indicated above, two equations are obtained from which the equations in part (b) of Table I may be derived (with the help of the information in Figs. 16 and 17) by solving for Z_{oe} and Z_{oo}.

The end sections, S_{01} and $S_{n,n+1}$, must be treated as a special case. Defining $Z_{\text{in}}(j\omega)$ as the impedance seen looking in the right end of the parallel-coupled section S_{01} in Fig. 1(a), with the left end connected to the input line of impedance Z_0, the following correspondences are forced with respect to $Z_{\text{in}}'(j\omega)$ indicated in Fig. 17:

(a) $\text{Re } Z_{\text{in}}(j\omega_0)=\text{Re } Z_{\text{in}}(j\omega_1)$ for the parallel-coupled terminating circuit, just as $\text{Re } Z_{\text{in}}'(j0)=\text{Re } Z_{\text{in}}'(-\omega_1')$ for the terminating circuit of the prototype.

(b) $\text{Im } Z_{\text{in}}(j\omega_1)/\text{Re } Z_{\text{in}}(j\omega_1)$ must equal $X'/R'=\text{Im } Z_{\text{in}}'(-j\omega_1')/\text{Re } Z_{\text{in}}'(-j\omega_1')$ computed from the prototype. (14)

Defining

$$P=\frac{(Z_{oe})_{01}-(Z_{oo})_{01}}{R_g 2\sin\theta_1}, \tag{15}$$

and

$$Q=\frac{(Z_{oe})_{01}+(Z_{oo})_{01}}{R_g 2\tan\theta_1}, \tag{16}$$

it can be shown that correspondence (a) in (14) will be obtained if

$$Q=\cot\theta_1 \tag{17}$$

[19] Taking $R_g=R_L=Z_0$.

is satisfied, where $\theta=\pi\omega_1/2\omega_0$. Further, correspondence (b) requires that

$$Q^3+Q(1-P^2)+\frac{X'}{R'}P^2=0 \tag{18}$$

be satisfied. Substituting (17) in (18), and solving for $(Z_{oe})_{01}$ and $(Z_{oo})_{01}$ yields the results in part (a) of Table I. Even if $R_g=Z_0$, the above conditions will generally result in an impedance level for $Z_{\text{in}}(j\omega)$ of the bandpass filter, which is different than that of $Z_{\text{in}}'(j\omega')$ for the prototype. The impedances of the interior sections must therefore be corrected by multiplying by the scale factor s indicated in Table I.

C. Procedure for Deriving the Equations in Table II

Fig. 18 shows the manner in which the modified prototype at (a) in Fig. 16 is broken into sections and the elements specified for deriving the equations in Table II. Note that in this case the end impedance inverters, K_{01} and $K_{n,n+1}$, are both made equal to the terminating resistances $R_g=R_L$. For the end inductances, $L_{a1}=L_{an}=R_g g_0 g_1$; however, $L_{a2}=L_{a3}=\cdots=L_{a,n-1}$ are made equal to $2L_{a1}$ so that the structure can be broken into symmetrical sections without the need for end sections. Using the indicated values for the L_{ak}, the $K_{k,k+1}$ are obtained by use of Fig. 16. Then all of the sections are designed by use of (9)–(12) and the correspondences given in (13).

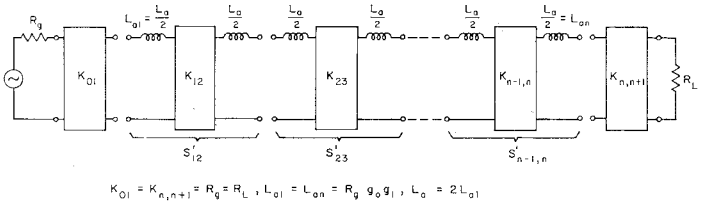

Fig. 18—Modified prototype for deriving the equations in Table II.

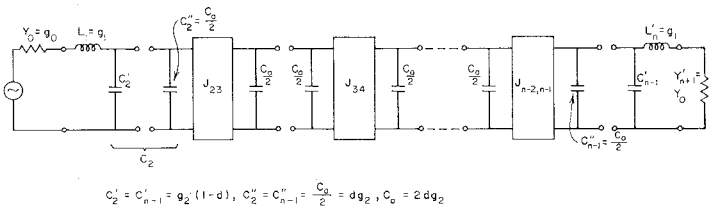

Fig. 19—Modified prototype for deriving the equations in Table III. Parameter d may be used to adjust the impedance level in the center part of the filter. In the example of Fig. 11, d was chosen as one-half, to split $C_2=C_2'+C_2''$ in half.

D. Procedure for Deriving the Equations in Table III

Fig. 19 shows the modified prototype used for deriving the equations in Table III. In this case, most of the structure is in the form shown in Fig. 16(b). However, inverters J_{01}, J_{12}, $J_{n-1,n}$, and $J_{n,n+1}$ have been omitted. Here, L_1 and C_2 have the same values that they had in

their original prototype form in Fig. 5. Capacitor C_2 is split into two parts, C_2' and C_2'', and the parameter d is used to establish what fraction of C_2 becomes C_2''. Then the capacitance values $C_{a3}=C_{a4}=\cdots=C_{a,n-2}$ are established, so that all of the interior sections can be broken into symmetrical sections. The interior sections are then related to parallel-coupled sections, as in Fig. 4(b) by dual procedures to those used for the interior sections for Tables I and II. The parallel-coupled sections are then converted to stub form by the equivalence in Fig. 4(b). The end sections are designed by forcing the stubs to have reactances at $\omega=\omega_0$ and $\omega=\omega_1$ (on a normalized basis) which are the same as those of the corresponding prototype elements L_1 and C_2', at $\omega'=0$ and $\omega'=-\omega_1'$, respectively.

This same general viewpoint should be useful for designing filters in the form in Fig. 1(c) and (d) to give some desired impedance level in the interior part of the filter. To accomplish this, the prototype in Fig. 18 should be converted to its dual form analogous to that shown in Fig. 16(a). Then, the capacitor C_1 is split, just as C_2 is split in Fig. 19. The resulting design equations are

$$C_a = 2dg_1, \qquad \frac{J_{12}}{Y_0}=\frac{J_{n-1,n}}{Y_0}=\frac{g_0\sqrt{g_1C_a}}{\sqrt{g_1g_2}},$$

$$\left.\frac{J_{k,k+1}}{Y_0}\right|_{k=2 \text{ to } n-2}=\frac{g_0C_a}{\sqrt{g_kg_{k-1}}},$$

$$M_{k,k+1}=\sqrt{\left(\frac{J_{k,k+1}}{Y_0}\right)^2+\left(\frac{g_0\omega_1'C_a\tan\theta_1}{2}\right)^2},$$

$$\left.Y^s_{k,k+1}\right|_{k=1 \text{ to } n-1}=Y_0\left(M_{k,k+1}-\frac{J_{k,k+1}}{Y_0}\right),$$

$$Y_1=Y_n=g_0Y_0\omega_1'(1-d)g_1\tan\theta_1+Y^s_{12},$$

$$\left.Y_k\right|_{k=2 \text{ to } n-1}=Y_{n-k+1}=Y^s_{k-1,k}+Y^s_{k,k+1},$$

$$\left.Y_{k,k+1}\right|_{k=1 \text{ to } n-1}=Y_{n-k,n-k+1}=J_{k,k+1}.$$

Although this technique has been used successfully for achieving small adjustments in impedance level within a filter, the filter-response accuracy resulting when this technique is used to achieve large changes in impedance level has not been tested.

E. Selection of Mapping Functions

Previous work of Cohn,[1] and also the plots presented herein, show that when the function in (4b) is used as indicated in Fig. 6 or 7 to map the response of a low-pass prototype, it will predict quite accurately the response of band-pass filters of the form in Fig. 1(a) having narrow or moderate bandwidth. Although the function in (4b) is very useful, it should not be expected to give high accuracy for wide-band cases because it is not periodic (which the filter response is), nor does it go to infinity for $\omega=0$, $2\omega_0$, $4\omega_0$, etc., which is necessary in order to predict the infinite attenuation frequencies in the response of the band-pass filter structure. It might at first seem that

$$F_n\left(\frac{\omega}{\omega_0}\right)=-\cot\left(\frac{\pi\omega}{2\omega_0}\right) \tag{19}$$

would solve this problem nicely, since it is periodic as desired, it varies similarly to (4b) in the vicinity of ω_0, and it has poles at the desired frequencies $\omega=0$, $2\omega_0$, $4\omega_0$, etc. However, if the structures in Fig. 1 are analyzed, it will be seen that no matter what value of n is used, the poles of attenuation at $\omega=0$, $2\omega_0$, $4\omega_0$, etc., *are always first-order poles*.[20] Meanwhile, an n-reactive-element prototype as in Fig. 5 (which will have an nth-order pole at $\omega'=\infty$) will map so as to give nth order poles at $\omega=0$, $2\omega_0$, etc., if the function in (19) is used. This important source of error is corrected in the case of (4a) by replacing $\cot(\pi\omega/2\omega_0)$ by $\cos(\pi\omega/2\omega_0)/|\sin(\pi\omega/2\omega_0)|$, and then taking the nth root of the denominator. In this manner, the poles generated by the zeros of $|\sin(\pi\omega/2\omega_0)|$ become of $1/n$ order, which causes the nth-order pole at $\omega'=\infty$ for the prototype response to map into first-order poles of the band-pass filter response at the desired frequencies.

In the case of the circuit in Fig. 3, the poles of attenuation at $\omega=0$, $2\omega_0$, $4\omega_0$, etc., will again always be of first order regardless of the value of n used. However, the series stubs at each end produce second-order poles at the frequency ω_∞ and at other corresponding points in the periodic response.[21] Thus, the

$$\sqrt[n]{|\sin(\pi\omega/2\omega_0)|}$$

factor in the denominator of (5) assures that the nth-order poles at $\omega'=\infty$ in the prototype response will always map to first-order poles at $\omega=0$, $2\omega_0$, etc., for the band-pass filter response. In addition, the factor

$$\sqrt[n]{\left[\sin\left(\frac{\pi}{2}\frac{(\omega-\omega_\infty)}{\omega_0}\right)\right]^2\left[\sin\left(\frac{\pi}{2}\frac{(\omega-2\omega_0+\omega_\infty)}{\omega_0}\right)\right]^2}$$

is introduced to cause the nth-order pole at infinity in the prototype response to map to second-order poles at ω_∞ (and other periodic points) for the band-pass filter

[20] For example, for the filter form in Fig. 1(d), as $\omega\to0$ the effect of all of the shunt stubs can be reduced to that of a single shunt zero-impedance branch which would produce a first-order pole of attenuation $\omega=0$. (One way in which higher-order poles can be generated is to produce shunt zero-impedance branches alternating with series branches having infinite impedance.)

[21] This can be seen as follows: For $\omega=\omega_\infty$, each of the series stubs represents an infinite-impedance series branch. For this single frequency, the interior part of the filter can be replaced by an equivalent T-section with a finite shunt impedance. Thus, the structure can be reduced (for the frequency ω_∞) to two series infinite-impedance branches separated by a finite shunt-impedance branch. This can be seen to result in a second-order pole of attenuation. (If the impedance of the equivalent shunt branch had been zero, the pole of attenuation would have been raised to third order.)

response. In this manner, all of the proper poles of attenuation are introduced with their proper order.

These principles can also be applied to the structure in Fig. 2, but this structure presents some new difficulties. It can be seen that this structure will develop nth-order poles of attenuation at ω_∞ and corresponding periodic points, but the half-wavelength stubs also introduce additional natural modes of oscillation which create, in addition to the desired pass band, a low-pass pass band (and corresponding periodic pass bands) as shown in the response in Fig. 10. This additional low-pass pass band approaches ω_∞ quite closely, with the result that, although the pole at ω_∞ is of relatively high order, its effectiveness is weakened by the close proximity of this low-pass pass band. The function

$$F_n\left(\frac{\omega}{\omega_0}\right) = \tan\left(\frac{\pi\omega}{\omega_0}\right) \tag{20}$$

for the case of $\omega_\infty/\omega_\infty = 0.50$ would map the prototype response to give a low-pass pass band, an nth-order pole at ω_∞, and the desired pass band centered at ω_0. However, it would not properly predict how close the low-pass pass band comes to ω_∞, nor could it account for the oversize attenuation ripples which occur in this band (Fig. 10). As a result, the function in (20) predicts an overly optimistic rate of cutoff at the edges of the pass band centered at ω_0. It is probable that a useful approximation could be obtained by using a mapping function, such as that in (20), with additional factors added which create zeros in $F_n(\omega/\omega_0)$, close to, but somewhat off, the $j\omega$ axis (regarded from the complex-frequency point of view). Proper location of these zeros could then be used to extend the low-pass pass band upwards toward ω_∞, which should give the proper effect.

TABLE I

DESIGN EQUATIONS ESPECIALLY SUITED FOR FILTERS OF THE FORM IN FIG. 1(a) AND (b)

Use mapping (4a) or (4b) and Fig. 6 or 7 to select prototype having required value of n. Equations below are for filters in the form of Fig. 1(a). There are $n+1$ parallel-coupled sections for an n-reactive-element prototype when using the design procedure below.

(a) Sections S_{01} and $S_{n,n+1}$

$$\frac{K_{01}}{Z_0} = \frac{1}{\sqrt{g_0 g_1 \omega_1'}} = \frac{K_{n,n+1}}{Z_0}, \qquad \theta_1 = \frac{\pi\omega_1}{2\omega_0}$$

$$Q = \cot\theta_1, \qquad P = \sqrt{\frac{Q(Q^2+1)}{Q + \dfrac{1}{2(K_{01}/Z_0)^2}}}$$

$$s = Z_0\left(\frac{P\sin\theta_1}{K_{01}/Z_0}\right)^2$$

$$(Z_{oe})_{01} = (Z_{oe})_{n,n+1} = Z_0(1 + P\sin\theta_1)$$

$$(Z_{oo})_{01} = (Z_{oo})_{n,n+1} = Z_0(1 - P\sin\theta_1)$$

(b) Sections S_{12} to $S_{n-1,n}$

$$\frac{K_{k,k+1}}{Z_0} = \frac{1}{\omega_1'\sqrt{g_k g_{k+1}}}, \qquad N_{k,k+1} = \sqrt{\left(\frac{K_{k,k+1}}{Z_0}\right)^2 + \frac{\tan^2\theta_1}{4}}$$

$$(Z_{oe})_{k,k+1} = (Z_{oe})_{n-k,n-k+1} = s\left(N_{k,k+1} + \frac{K_{k,k+1}}{Z_0}\right)$$

$$(Z_{oo})_{k,k+1} = (Z_{oo})_{n-k,n-k+1} = s\left(N_{k,k+1} - \frac{K_{k,k+1}}{Z_0}\right)$$

where θ_1 and s are defined as in (a) above and $k = 1, 2, \cdots, n-1$.

TABLE II

DESIGN EQUATIONS FOR FILTERS ESPECIALLY SUITED FOR REALIZATION IN THE FORM IN FIG. 1(c) AND (d)

Use mapping (4a) or (4b) and Figs. 6 or 7 to select prototype. Equations below are for filters in the form of Fig. 1(a), but they are readily converted to the form in Fig. 1(c) or (d) by use of Fig. 4. Using these equations, sections S_{01} and $S_{n,n+1}$ are omitted, and there will be $n-1$ parallel-coupled sections for an n-reactive-element prototype.

Sections S_{12} to $S_{n-1,n}$

$$\frac{K_{12}}{Z_0} = \frac{K_{n-1,n}}{Z_0} = \frac{\sqrt{2}g_0 g_1}{\sqrt{g_1 g_2}},$$

$$\left.\frac{K_{k,k+1}}{Z_0}\right|_{k=2 \text{ to } n-2} = \frac{K_{n-k,n-k+1}}{Z_0} = \frac{2g_0 g_1}{\sqrt{g_1 g_k g_{k+1}}},$$

$$\theta_1 = \frac{\pi}{2}\frac{\omega_1}{\omega_0}, \qquad N_{k,k+1} = \sqrt{\left(\frac{K_{k,k+1}}{Z_0}\right)^2 + (\omega_1' g_0 g_1 \tan\theta_1)^2}$$

$$(Z_{oe})_{k,k+1} = (Z_{oe})_{n-k,n-k+1} = Z_0\left(N_{k,k+1} + \frac{K_{k,k+1}}{Z_0}\right)$$

$$(Z_{oo})_{k,k+1} = (Z_{oo})_{n-k,n-k+1} = Z_0\left(N_{k,k+1} - \frac{K_{k,k+1}}{Z_0}\right)$$

where $k = 1, 2, \cdots, n-1$.

TABLE III

DESIGN EQUATIONS FOR FILTERS OF THE FORM IN FIG. 3

Use mapping (5) and Fig. 6 or 7 to select prototype.

$$\theta_1 = \frac{\pi\omega_1}{2\omega_0}, \qquad \theta_\infty = \frac{\pi\omega_\infty}{2\omega_0},$$

where ω_∞ is a frequency of infinite attenuation as indicated in Fig. 11. Referring to Fig. 3:

$$a = \cot^2\theta_\infty, \qquad Z_1 = Z_n = \frac{[a(\tan\theta_1)^2 - 1]\omega_1' g_0 g_1}{Y_0(a+1)\tan\theta_1},$$

$$Z_1' = Z_n' = aZ_1, \qquad C_a = 2dg_2,$$

where $d \leq 1$ is a constant (typically one-half or somewhat larger), which may be chosen to give a desired impedance level in the interior of the filter.

$$\frac{J_{23}}{Y_0} = \frac{J_{n-2,n-1}}{Y_0} = \frac{\sqrt{g_2 C_a}}{g_0\sqrt{g_2 g_3}}, \qquad \left.\frac{J_{k,k+1}}{Y_0}\right|_{k=3 \text{ to } n-3} = \frac{C_a}{g_0\sqrt{g_k g_{k+1}}},$$

$$M_{k,k+1} = \sqrt{\left(\frac{J_{k,k+1}}{Y_0}\right)^2 + \left(\frac{\omega_1' C_a \tan\theta_1}{2g_0}\right)^2},$$

$$\left.Y^s_{k,k+1}\right|_{k=2 \text{ to } n-2} = Y^s_{n-k,n-k+1} = Y_0\left(M_{k,k+1} - \frac{J_{k,k+1}}{Y_0}\right).$$

Then for the shunt stubs:

$$Y_2 = Y_{n-1} = \frac{Y_0\omega_1'(1-d)g_2}{g_0}\tan\theta_1 + Y^s_{22},$$

$$\left.Y_k\right|_{k=3 \text{ to } n-2} = Y_{n-k+1} = Y^s_{k-1,k} + Y^s_{k,k+1}.$$

And for the connecting lines:

$$\left.Y_{k,k+1}\right|_{k=2 \text{ to } n-1} = Y_{n-k,n-k+1} = J_{k,k+1}.$$

TABLE IV

SUMMARY OF EVEN-MODE AND ODD-MODE IMPEDANCE VALUES FOR THE FILTERS OF FIG. 8(a)–(c) DESIGNED BY USE OF TABLE I AND REALIZED IN THE FORM IN FIG. 1(a)

	Fig. 8(a) (5% Bandwidth)	Fig. 8(b) (30% Bandwidth)	Fig. 8(c) (2 to 1 Bandwidth)
$(Z_{oe})_{01}=(Z_{oe})_{67}$	1.251	1.540	1.716
$(Z_{oe})_{12}=(Z_{oe})_{56}$	0.996	1.023	1.142
$(Z_{oe})_{23}=(Z_{oe})_{45}$	0.981	0.937	0.954
$(Z_{oe})_{34}$	0.980	0.927	0.933
$(Z_{oo})_{01}=(Z_{oo})_{67}$	0.749	0.460	0.284
$(Z_{oo})_{12}=(Z_{oo})_{56}$	0.881	0.491	0.208
$(Z_{oo})_{23}=(Z_{oo})_{45}$	0.895	0.536	0 250
$(Z_{oo})_{44}$	0.896	0.542	0.255

All values normalized so that $Z_o=1$.

TABLE V

ELEMENT VALUES FOR THE FILTER OF FIG. 9 REALIZED AS SHOWN IN FIG. 1(d)

Filter designed using Table II from a 0.10-db ripple, $n=8$, Tchebycheff prototype using $\omega_1/\omega_0=0.650$.

$Y_1=Y_8=1.042$	$Y_3=Y_6=2.049$
$Y_{12}=Y_{78}=1.288$	$Y_{34}=Y_{56}=1.292$
$Y_2=Y_7=2.050$	$Y_4=Y_5=2.087$
$Y_{23}=Y_{67}=1.364$	$Y_{45}=1.277$

All values normalized so $Y_0=1$.

TABLE VI

ELEMENT VALUES FOR THE FILTER OF FIG. 10 REALIZED AS SHOWN IN FIG. 2

Filter designed from a 0.10-db ripple, $n=8$, Tchebycheff prototype using $\omega_1/\omega_0=0.850$ and $\omega_\infty/\omega_0=0.500$. This, then, calls for $a=1$ so that $Y_k'=Y_k''$ throughout.

$Y_1'=Y_8'=1.806$	$Y_3'=Y_6'=3.584$
$Y_{12}=Y_{78}=1.288$	$Y_{34}=Y_{56}=1.292$
$Y_2'=Y_7'=3.585$	$Y_4'=Y_5'=3.614$
$Y_{23}=Y_{67}=1.364$	$Y_{45}=1.277$

All values normalized so that $Y_0=1$.

TABLE VII

ELEMENT VALUES FOR THE FILTER OF FIG. 11 REALIZED AS SHOWN IN FIG. 3

Filter designed using Table III from a 0.10-db ripple, $n=8$, Tchebycheff prototype using $\omega/\omega_0=0.650$ and $\omega_\infty/\omega_0=0.500$.

$Z_1=Z_8=0.606$	$Y_3=Y_6=1.235$
$Z_1'=Z_8'=0.606$	$Y_{34}=Y_{56}=0.779$
$Y_2=Y_7=1.779$	$Y_4=Y_5=1.258$
$Y_{23}=Y_{67}=0.823$	$Y_{45}=0.770$

Radio-Frequency System of the Cambridge Electron Accelerator*

KENNETH W. ROBINSON†, MEMBER, IRE

Summary—**The requirements for the RF system of the Cambridge Electron Accelerator are investigated and the choice of the major parameters of the system is discussed. The strongly coupled waveguide cavity system is analyzed and the performance of the system with various types of imperfections is calculated.**

INTRODUCTION

THE Cambridge Electron Accelerator is a project to design and construct a 6-billion-volt electron synchrotron at Harvard University to be used for high energy physics research.[1]

The Cambridge accelerator has two important differences from most synchrotrons which require the design of the RF system to be very different from that of other circular accelerators. The electrons radiate electromagnetic energy due to the curvature of their orbits in the magnetic guide field. At 6 bev, the radiation loss is 4.5 mev per turn. This radiation loss occurs as discrete quanta which are typically 15-kv X rays at 6 bev. The emission of these discrete quanta produces synchronous oscillations of the individual electrons in energy and phase position about the equilibrium values, and requires the RF voltage to be substantially larger than the radiation loss, in order to prevent the particles being lost from the phase stable region.[2] The other characteristic is the initial injection of electrons at an energy of 20 mev or higher which eliminates the need to modulate the frequency, and makes it possible to use high Q cavities for the system.

The problem of the RF system is, then, to design a system capable of developing the large accelerating voltage required to make up the peak radiation loss of 4.5 mev per turn and contain the quantum induced phase oscillations. During the acceleration cycle the radiation

* Received by the PGMTT, April 14, 1960; revised manuscript received July 13, 1960.

† Cambridge Electron Accelerator, Harvard University, Cambridge, Mass.

[1] *Proc. Internatl. Conf. on High-Energy Accelerators and Instrumentation*, CERN, Geneva, Swiz., pp. 335–338; 1959.

[2] M. Sands, "Synchroton oscillations induced by radiation fluctuations," *Phys. Rev.*, vol. 97, pp. 470–473; 1955.